THESIS

DISCOVERY AND PROPERTIES OF HYBRID MATERIALS FOR POTENTIAL APPLICATIONS IN QUANTUM INFORMATION SCIENCE

Submitted by

Crystal J. Lundgren

Department of Chemistry

In partial fulfillment of the requirements

For the Degree of Master of Science

Colorado State University

Fort Collins, Colorado

Fall 2022

Master's Committee:

Advisor: James R. Neilson

Amy Prieto
Kristen Buchanan

ABSTRACT

DISCOVERY AND PROPERTIES OF HYBRID MATERIALS FOR POTENTIAL APPLICATIONS IN QUANTUM INFORMATION SCIENCE

Hybrid halide perovskites and their derivatives are sought after for their unique optoelectronic properties, ease of preparation, and highly tunable structure. Some conjugated π-system containing hybrid halide semiconductors derived from hybrid perovskites show a unique primary electronic transition from the inorganic layer (halide) states to the organic layer (π^*) states. This type of charge-transfer semiconductor demonstrates a quantum two-level system between these frontier orbitals, suggesting that these materials may be useful as qubits in quantum computation. For a material to be suitable for a qubit, it must contain a quantum two-level system that can be characterized via optically adressable emission. Here, a new family of hybrid halide semiconductors containing 4-amino-1,2,4-triazole (4AMTZ) are discovered. Chapter 2 discusses the synthesis and characterization of 4AMTZBiI_4. The crystal structure of 4AMTZBiI_4 is solved and confirmed with powder X-ray diffraction. Photoluminescence studies reveal that there is no optically addressable emission from this system, and the iodide congener is thus not usable as a qubit. Chapter 3 discusses the synthesis and photoluminescence emission spectra of 4AMTZBiBr_4 and 4AMTZBiCl_4. These studies reveal emission from both the chloride and bromide congeners at T = 77 K that is likely due to the primary charge transfer between the halide and organic states based on the blue shifting of 4AMTZBiBr_4 (475 nm) relative to that of 4AMTZBiCl_4 (415 nm). Another region of emission observed in both 4AMTZBiBr_4 and 4AMTZBiCl_4 is centered at 660 nm. This region of emission is not shifted between the halide congeners, suggesting the presence of an emissive self-trapped exciton localized on the inorganic lattice. Though these materials emit at T=77K, there is no optically addressable emission at room temperature.

ACKNOWLEDGEMENTS

Thank you to Jamie Neilson and the CSU Analytical Resources Core for supporting this project.

DEDICATION

For Clyde, you are a good cat when you aren't biting me.

TABLE OF CONTENTS

LIST OF FIGURES

Chapter 1

Introduction

1.1 Tunability of Organic-Inorganic Hybrid Perovskites

The term "perovskite" refers to the mineral $CaTiO_3$. Solid state chemists, however, use perovskite to describe a family of materials with the structural formula of the traditional perovskite, ABX_3. Adjusting the components used for the "A", "B", and "X" sites can result in a material that strays from the ABX_3 structure, but is still captured under the perovskite umbrella.

Most organic-inorganic hybrid perovskites stem from the traditional perovskite structure. In hybrid structures, the "A" site is typically an organic cation, the "B" site is a metal, and the "X" site is a halide. These structures are layered, with the organic cation acting as a spacer between layers of inorganic metal halides. Substitution of the "A", "B", and "X" sites with different cations, metals, and halides results in unique structures that differ from the traditional perovskite, though they all consist of alternating inorganic and organic layers. Because these hybrid materials are structurally dependent on the type of "A", "B", and "X" site material used, their resulting optoelectronic properties are highly tunable.

Tunability of optoelectronic properties is a desirable quality to have in materials used for lighting, displays, and quantum information science. There are several mechanisms for light emission in a hybrid perovskite or derivative that are easily tuned by manipulation of the "A" and "X" sites. Incorporating cyclical organic cations that contain conjugated π systems onto the "A" site of the hybrid perovskite often results in the formation of a charge transfer semiconductor, which usually adopt more complex structures than the traditional ABX_3 perovskite. In this type of semiconductor the frontier electronic states are composed of the halide states (valence band maximum) and organic states (conduction band minimum).

Figure 1.1 shows the densities of states (DOS) for the hybrid charge-transfer semiconductors $(C_7H_7)SbI_4$ and $(C_7H_7)BiI_4$. The choice of metal shows some effect on the bandgap, with a slight

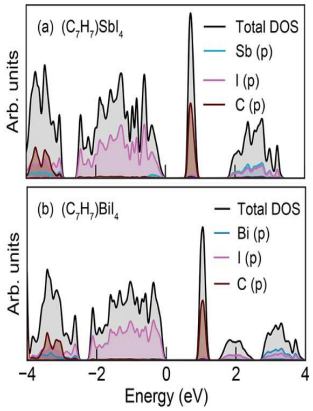

Figure 1.1: Density of states plotted for two charge-transfer semiconductors $(C_7H_7)SbI_4$ and $(C_7H_7)SbI_4$. [1]

increase in bandgap energy in the bismuth containing material as opposed to the antimony containing material. Since the valence band maximum is highly dependent on halide states with negligible contribution from the "B" site metal, the bandgap energy may be tuned by adjusting the "X" site halide.

Aside from the halide present on the X site, there is opportunity to tune emission by adjusting the organic spacer cation present on the A site. Self trapped excitons (STEs) consist of a bound electron-hole pair with a binding energy equal to K_bT, where K_b is the Boltzmann proportionality constant and T is the temperature of the system. Excitons are considered to be "self-trapped" when they induce distortions in the inorganic lattice creating a "quantum well" where they are localized. Often, STEs are localized on the inorganic octahedra of hybrid materials. The energy of the quantum well, and thus the emission energy, is dependent on the tilt angle of the inorganic octahedra, which can be manipulated by adjusting the size and length of the organic spacer cation [2, 3]. The ability to tune the optoelectronic properties in charge transfer and STE mechanisms via "A" and "X" site manipulation is desirable for designing materials that emit light in a specific region. This concept can be carried over to quantum information science and the development of qubits, as the ability to readout and initialize the quantum states is necessary to imbue information into those states.

1.2 Qubits and Quantum Information Science

Extending computation to the quantum realm is the emerging next level of information processing that will result in greater computational power than is currently accessible from classical bits. Employing quantum bits, or "qubits", to imbue computational memory relies on two-dimensional vector space within the quantum system [4,5]. Because the qubit has access to quantum states, it is able to sample a near infinite number of solutions at a time, where classical bits are only capable of being in two states, 0 or 1. This access to nearly infinite states allows complex computations that require multiple steps to be performed with greater efficiency. Processes such as random number generation and integer factorization can be optimized, and other complex multi-step computations are able to be completed under a practical timescale that cannot be achieved by a classical computer. Certain criteria must be met for a material to be suitable for a qubit. The qubit must be a well characterized quantum two-level system, be able to be initialized into a known state, have a suitably long coherence time, be specifically measurable, and satisfy universal quantum gates [4–6].

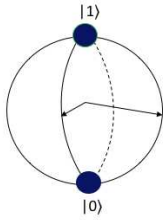

Figure 1.2: Schematic of a well characterized quantum two-level system. $|0\rangle$ and $|1\rangle$ represent the two "known" states the system can be in (i.e. ground state and excited state). Between these two states is a two dimensional vector space with a nearly infinite number of states the qubit could potentially occupy.

.

Materials that contain an optically addressable two-level quantum system are desirable for use as qubits, as qubits rely on the two-dimensional vector space between the two states to sample a nearly infinite number of solutions at once. The ability to control and characterize the excited electronic states of the qubit is essential to reading out information from the system of qubits, as well as to initialize the qubit into a known state before computation can begin. Initialization into a known state and characterization of the excited electronic states relies on optoelectronic emission

from the material. This two-level vector space and ability to readout and manipulate the two level state are two of the most basic criteria for a functional qubit [4]. Many well characterized two level systems are being investigated for their potential role in quantum information science. These systems include spin relaxation complexes [6–8], quasi-particles such as excitons [9–11], and the defect centers in solid state materials [9, 12–14]. Hybrid halide perovskites and their derivatives are a natural extension of qubit research, given their propensity for easily tunable STE and charge transfer properties.

1.3 Photoluminescence Spectroscopy

Photoluminescence spectroscopy can be used to investigate the optoelectronic properties of solid state materials in a quick and non-destructive manner. When applying photoluminescence studies to materials we wish to use as qubits, we must consider the emission, excitation, and quantum yield together. Emission occurs when excited states are populated with a wavelength of sufficient energy, photons then relax from the excited state, emitting excess energy. An excitation spectrum can be taken by probing the expected emission wavelength and plotting the wavelengths of light that result in that emission. This gives useful information about how the material may be induced into the excited state so that emission can occur. The efficiency of emission for a material can be described using quantum yield, which is calculated as a ratio of the number of photons emitted to the number of photons absorbed, often reported as a percent.

Given that base criteria for a qubit includes the ability to initialize the material into a known state, as well as the ability to readout information from that state, high quantum yield and knowledge of the excitation and emission spectra are essential. Using an excitation spectrum, it is possible to determine an exact wavelength of light that will most efficiently populate the excited states of the material. In other words, we can initialize the material into a "known" excited state with a single pulse of light, fulfilling that criteria. The emission spectrum is important for manipulation and readout of the qubit. Well characterized emission spectra demonstrate which wavelength of light is ideal for populating excited states, as well as what energy of light the material typically

emits after these states have been populated. Materials with quantum high quantum yields and a known emission range can be further studied for qubit suitability with methods such as optically detected magnetic resonance.

1.4 Optically Detected Magnetic Resonance

Optically detected magnetic resonance (ODMR) is a spectroscopy method used to investigate the electronic states of emitting materials. While in the excited, usually triplet, state electrons are typically paramagnetic. Using magnetic and microwave fields, the spin state of these electrons can be exploited to determine the hyperfine interactions of the excited electrons and their local environment. Application of resonant microwaves to the excited triplet state will cause the populations among the excited triplet sublevels to change. Since the optical emission of a material is dependent on the population of the excited states there will be a subsequent change in the emission spectrum reflecting the new sublevel populations. Monitoring the change in photoluminescence spectra for emitting materials can yield important information about the spin states of the electrons as well as how the spin states are interacting with the environment. ODMR is a highly sensitive method since it uses the optoelectronic properties, which are relatively high energy, to determine the magnetic properties of the material [15]. Because quantum computation relies on the ability to coherently control and readout the electronic state of the qubit, ODMR is an important method for screening materials for their suitability as qubits.

Chapter 2

DISCOVERY AND PROPERTIES OF 4-amino-1,2,4-triazolium Bismuth Iodide

2.1 Introduction

Given the tunable nature of hybrid materials, there is rich scientific potential in the exploration of new materials. Particularly, exploration of layered hybrid halide structures containing cyclical organic cations that contain conjugated π systems due to their propensity for charge transfer between their frontier electronic states. Further tuning of the valence band maximum is possible by adjusting the species of halide present in the inorganic octahedra due to this frontier orbital being composed of halide states. Emission from either this kind of charge-transfer or a STE will indicate that the material is a candidate for use as a qubit. Studies using ODMR to characterize the hyperfine electronic interactions can be utilized to further address the material's suitability for quantum information.

A class of bismuth halide hybrid semiconductors containing the cyclical conjugated π system cation $C_7H_7^+$ (tropylium) is reported to show charge transfer between the frontier electronic states [1], though no photoluminescence of these materials has been published. Adjustment of the organic cation in these materials has potential to alter the optoelectronic emission by two different mechanisms: band gap energy and STE. The conduction band minimum in these materials is reported to be composed of organic cation states [1], so adjusting the energy level of the organic cation can alter the bandgap energy that this electronic transition occurs across. The presence of a STE may be induced via alteration of the organic spacer cation. Since STEs localize on the inorganic octahedra and have an emission energy relative to the quantum well they are trapped in, we may use the organic spacer cation to adjust the energy level of the quantum well by influencing

the octahedral tilt of the inorganic layer [3]. Both of these mechanisms are easily accessible when investigating the solution processable hybrid halide semiconductors.

This thesis discusses a family of bismuth iodide based hybrid semiconductors containing the conjugated π system 4-amino-1,2,4-triazolium (4AMTZ) as the organic spacer cation. The structure of 4AMTZBiI_4 is determined using single crystal and powder X-ray diffraction. Density of states calculations are performed using the solved structure of 4AMTZBiI_4 to determine the frontier electronic states. Low-temperature (T=77 K) and room temperature photoluminescence emission spectra are collected to determine the optoelectronic properties of the materials.

2.2 Experimental

2.2.1 Starting Materials

Bismuth(III) oxychloride (98%, Sigma Aldrich), 4-amino-1,2,4-triazole (99%, Sigma Aldrich), acetic acid (glacial, certified ACS, Fisher Chemical), ethyl ether (anhydrous, Fischer Chemical), and hydroiodic acid (57 wt. $\%$ in H_2O, distilled, H_3PO_2 stabilized, 99.95 $\%$, Sigma Aldrich) were purchased from stated commercial suppliers and used without further purification.

2.2.2 Synthesis of 4-amino-1,2,4-triazolium Bismuth Iodide Powder

Bismuth(III) oxychloride (2.1 g, 8.0 mmol) was added to 5.0 mL hydroiodic acid and stirred at room temperature until dissolved to make Bi^{3+} stock solution (1.6 mM). 4AMTZ (0.72 g, 8.5 mmol) was added to 2 mL hydroiodic acid and stirred at room temperature until dissolved. Upon adding the two solutions a dark red precipitate formed in a bright red solution. Acetic acid (2.0 mL) was added as an antisolvent to increase yield and the solution was allowed to stir for 15 minutes. The resulting red solid was filtered, washed with acetic acid, and dried under vacuum at room temperature overnight. The solid is identified as 4-amino-1,2,4-triazolium bismuth iodide, 4AMTZBiI_4.

2.2.3 Single Crystal Growth

A sample from the bulk powder of prepared 4AMTZBiI$_4$ (0.2305 g), was placed into a glass vial with a magnetic stir bar and 2 mL of hot acetic acid. Hydroiodic acid was filtered with a 45 μm pore size 25 mm diameter polypropylene syringe filter and added to the vial dropwise, with stirring, until the solid was just dissolved. The sample was then allowed to slow cool to room temperature overnight. The resulting crystals were filtered and washed with diethyl ether. A clear, well defined single crystal with regular geometry and no visible color variation was selected for single crystal X-ray diffraction. The remaining crystals were ground into a powder to be used for powder X-ray diffraction.

2.2.4 Single Crystal X-Ray Diffraction

Single crystal X-ray diffraction data was collected on a Bruker D8 Quest diffractometer with a Mo Kα radiation source and Photon 50^{TM} CMOS detector. A single crystal of 4AMTZBiI$_4$ was mounted on a MiTeGen tip with paratone oil. Data were collected at T= 250 K. APEX3 software was used to reduce and integrate the single crystal data. XPREP was used to load the data and create a starting model for the crystal structure using SHELXT software.

2.2.5 Powder X-Ray Diffraction

Powder X-ray diffraction measurements were carried out using a Bruker D8 DaVinci Diffractometer with a Cu Kα radiation source and LYNXEYE-EX-T energy discriminating detector. Samples were prepared using a zero diffraction silicon wafer. A sample of powdered 4AMTZBiI$_4$ single crystals were dusted over a small amount of petroleum jelly. TOPAS software was used to refine the data based on the crystal structure generated from the single crystal X-ray diffraction data in the orthorhombic space group Pbca (No. 61).

2.2.6 DFT Calculations

The densities of states (DOS) for 4AMTZBiI$_4$ was calculated using the vienna ab initio software package (VASP) executables with the summit research supercomputer at CU Boulder. Struc-

tural information about 4AMTZBiI$_4$ was based upon the crystal structure (Figure 2.1). An initial calculation was completed without including the partial contribution of each orbital to the DOS. For this calculation, a self consistent calculation was run using a k-point mesh of 6x4x4 generated using the Monkhorst-Pack scheme to establish a charge density from which the total DOS could be plotted and serve as a basis for future calculations, the energy cutoff was 540 eV. Using a k-point mesh of 8x7x7, the partial DOS was calculated and visualized using sumo.

2.2.7 UV-Vis Spectroscopy

UV-Vis absorbance data was gathered with a OceanOptics HL-2000-FHSA tungsten halogen light source equipped with an integrating sphere. OceanView software was used to collect the data with an integration time of 1000 ms and 10 average scans.

2.2.8 Photoluminescence Spectroscopy

An Edinburgh FS5 spectrofluorometer with a 150 W xenon lamp light source was used for all photoluminescence spectroscopy measurements. The excitation and emission monochromator range was 200 - 1000 nm and the emission detection range was 230 - 870 nm. A solid sample holder was used for room temperature measurements. For low temperature (T= 77 K) measurements, the solid sample was placed in a clear thin wall quartz EPR sample tube before being slowly inserted into a low temperature sample stage filled with liquid nitrogen. Blanks were taken using an empty thin wall quartz tube as well as silica powder in a thin wall quartz tube.

2.3 Structural Characterization

Single crystal X-Ray diffraction shows that the hybrid semiconductor 4ATMZBiI$_4$ crystallize in the space group $Pbca$ (Figure 2.1). The inorganic layer consists of bismuth iodide octahedral dimers, the octahedra are trigonally distorted, with the z axis iodides bent at a less than 90°angle and distorted bond lengths. The octahedra are substantially tilted, and are nearly corner sharing be-

tween dimers. These layers of dimerized bismuth iodide octahedra are seperated by "herringbone" packed 4-amino-1,2,4-triazolium cations.

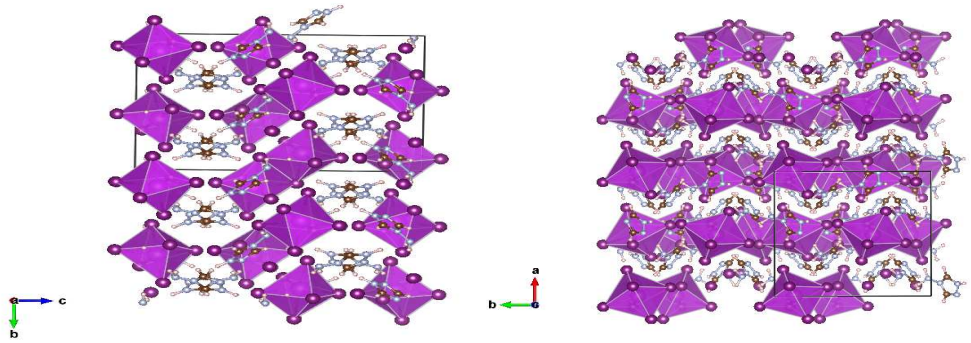

Figure 2.1: Crystal structure of $4AMTZBiI_4$ as shown looking down the a axis (left) and the c axis (right).

Both the amino headgroup as well as the 1 and 2 position nitrogens in the conjugated ring have the ability to be protonated when the 4-amino-1,2,4-triazole is dissolved in a hydrohalic acid (Figure 2.2). Which species is incorporated into the crystal structure, however, remains ambiguous. ChemAxon software was used to estimate the distribution of 4-amino-1,2,4-triazole microspecies based on the pH of the solution. At low pH protonation mainly occurs on an unsubstituted ring nitrogen, or the amino headgroup. These two species exist in the majority, with the ring protonated species slightly favored. Additionally, the ring nitrogen site is stabilized by resonance of the ring, and it is likely stable when being incorporated into the crystal structure. For these reasons, the triazolium structure that is protonated on the ring nitrogen is used in the single crystal model. Neutron diffraction experiments could be done in the future to resolve the precise location of the nitrogens in the crystal structure. In the case that both species of triazolium are present in the crystal structure, vibrational spectroscopy may be used to compare the stretching of the N-H bonds to add more clarity to the structure. For the purpose of determining the frontier electronic states, the exact location of the proton is negligible since the hydrogen states are not a major contribution to the valence or conduction band.

Powder X-ray diffraction data from powdered $4AMTZBiI_4$ single crystals is consistent with the solved crystal structure (Figure 2.3). PXRD of bulk powder samples did not fit the predicted

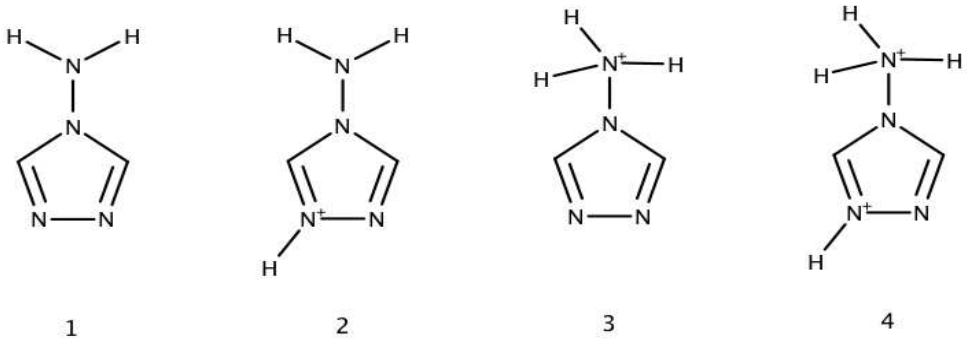

Figure 2.2: Schematic showing the various microspecies of 4-amino-1,2,4-triazole (1). Three protonation states may occur, on the ring nitrogen (2), the amino headgroup (3), or both sites resulting in a +2 charge cation (4).

pattern from the crystal structure, suggesting that the bulk powder samples contain multiple polymorphs or distinct compositions in this phase space. Deviations in intensity from the PXRD data and the expected pattern generated from the crystal structure are likely due to anisotropy of the heavy bismuth and iodide atoms in the structure. Reconstructing a structure from the PXRD data resulted in a structure with elongated Bi-I bonds and fragmented organic cations. The organic cations may be somewhat disordered in the crystal, but their positions will not significantly impact the diffraction due to the low relative atomic number of the constituent atoms. Likely, there is distortion in the main group elements. Nonetheless, we can determine from the PXRD data that the bulk specimen is single phase.

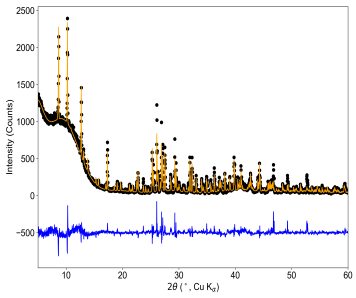

Figure 2.3: Rietveld refinement of powdered 4AMTZBiI_4 single crystals using the solved crystal structure shown in Figure 2.1. Yellow lines represent the predicted powder patter, black circles represent the collected data, and the blue line represents the difference curve.

2.4 Electronic Structure Calculations

The density of states shown in Figure 2.4 reveals that the valence band maximum is primarily composed of halide states from the inorganic octahedra and the conduction band minimum is primarily composed of localized carbon and nitrogen states. This confirms that the hybrid semiconductor $4AMTZBiI_4$ is a charge-transfer semiconductor with frontier states dependent on the organic and inorganic layers, with frontier states similarly composed to $C_7H_7^+$ bismuth iodide and $C_7H_7^+$ antimony iodide (Figure 1.1) [1]. The bandgap of this material ($\sim$2 eV), could be easily tuned to a higher energy by replacing the iodine with a smaller halide, such as chlorine or bromine.

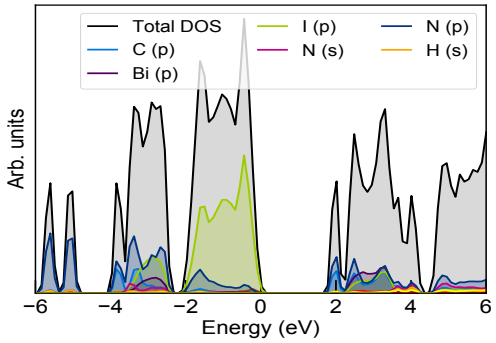

Figure 2.4: Density of states plotted for 4AMTZBiI4.

2.5 Optoelectronic Properties

The UV-Vis absorbance spectrum for $4AMTZBiI_4$ is shown in Figure 2.5. Peak absorbance at 600 nm (2.0 eV) is consistent with what we would expect for a bright red material. The absorbance covers most of the visible spectrum, and we would expect emission to occur at wavelengths >800 nm since materials emit at a lower energy than they absorb, due to the stokes shift that typically occurs.

Photoluminescence emission studies show no appreciable emission at room or low temperature for $4AMTZBiI_4$. Figure 2.7 shows the overlayed photoluminescence spectra for room temperature, low temperature, and empty thin wall quartz tube measurements. While there are distinct peaks in this spectrum, they do not represent emission from $4AMTZBiI_4$. This emission is consistent

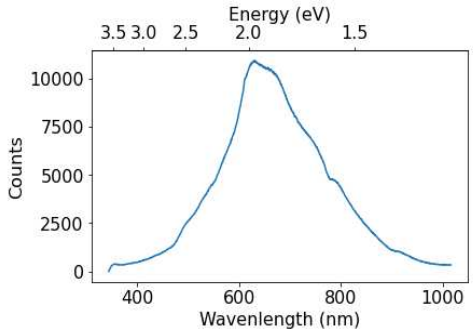

Figure 2.5: UV-Vis absorbance spectrum for 4AMTZBiI4.

with the emission from the xenon lamp, as evidenced with the close match to the spectrum taken from an empty tube. While there is a peak in both $4AMTZBiI_4$ spectra at 760 nm that is not present in the spectrum of the empty tube, Figure 2.6 shows the same spectra for low and room temperature $4AMTZBiI_4$ photoluminescence measurements overlayed with a silica blank. The increase in signal between 750 nm - 775 nm from the silica blank suggests that the peak in the $4AMTZBiI_4$ emission spectrum is due to scattering of the xenon emission by the powder, but is not emission from $4AMTZBiI_4$.

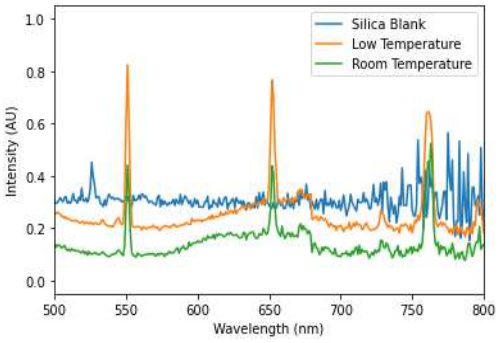

Figure 2.6: Photoluminescence emission for $4AMTZBiI_4$ at room temperature (green), low temperature (T=77 K) (orange), and a silica blank (blue).

The lack of strong emission in this spectrum indicates that there is no optically-addressable emission mechanism, either from charge-transfer or a self trapped exciton, meaning this material is not suitable for further studies with ODMR and cannot be used as a qubit.

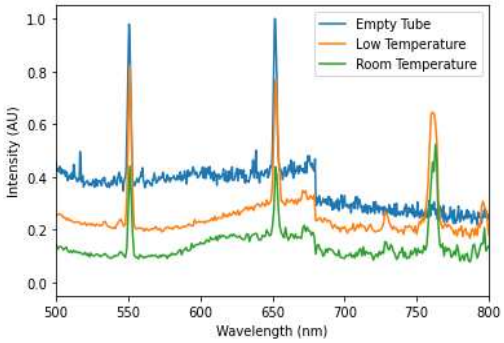

Figure 2.7: Photoluminescence emission for 4AMTZBiI4 at room temperature (green), low temperature (T=77 K) (orange), and an empty thin wall quartz EPR tube (blue).

2.6 Conclusion

The hybrid semiconductor 4AMTZBiI_4 is a charge-transfer semiconductor composed of alternating layers of bismuth iodide octahedra and 4-amino-1,2,4-triazolium cations, that crystallizes in the space group $Pbca$. The frontier orbitals are, like other conjugated π system containing hybrid materials, composed of halide states (valence band maximum) and organic states (conduction band minimum) with a calculated band gap of around 2 eV. While this material shows the electronic structure of a charge transfer semiconductor, it does not show optically addressable emission at room temperature or T=77 K. Further, there is no evidence of emission from a self-trapped exciton in the photoluminescence spectra. Because this material does not show optically addressable emission, it is not a candidate for a qubit.

The most basic critera for a qubit is that the material contains an optically addressable quantum two-level system [4]. Though the charge transfer between the frontier electronic states in 4AMTZBiI_4 is a quantum two-level system, there is no optically addressable emission from this system. While 4AMTZBiI_4 is not suitable for a qubit, there is ample opportunity to tune this material to be an optically active emitter. Future work should include studies of 4-amino-1,2,4-triazolium bismuth halide materials containing either chlorine or bromine to increase the bandgap energy. Incorporating other organic π system containing cations into bismuth iodide materials may also yield optically addressable emission either by emission from charge transfer or by inducing STE on the inorganic lattice by maximizing octahedral tilt angle [3].

Chapter 3

Optoelectronic Properties of 4AMTZBiCl$_4$ and 4AMTZBiBr$_4$

3.1 Introduction

Discovery of a hybrid semiconductor suitable for use as a qubit in quantum computation relies on synthesizing a material that demonstrates an optically active quantum two-level system. A charge transfer hybrid semiconductor where the primary electronic transition occurs between the valence and conduction bands is a good candidate for a qubit since the transition from valence to conduction band is a well characterized quantum two-level system. $C_7H_7^+$ (tropylium) containing hybrid halide charge transfer semiconductors $(C_7H_7)_2PbI_6$ and $C_7H_7BiX_4$ (X = Cl, Br, I) have been shown to contain a charge transfer from the halide states to the organic cation states [1, 16]. Tropylium is an organic cation that contains a conjugated pi system with a delocalized positive charge within a seven membered ring. The unique access to pi states introduced by this cation allows access to π^* organic states, facilitating this π to π^* transition.

Because of the dependence of the valence band maximum on halide states, the bandgap of these materials are easily tunable. Adjusting the energy level of the valence band (i.e. switching the halide) while keeping the energy level of the organic cation π^* states the same results in a bandgap energy that is directly related to the chosen halide. In the case of $C_7H_7BiX_4$ (X = Cl, Br, I), the bandgap is shown to decrease as halide size increases [1]. Since the p orbital energy of the halide, which make up the valence band maximum, increases a halide size increases, this trend is expected. There is also a slight increase in the bandgap energies of $C_7H_7BiX_4$ compared to $C_7H_7SbX_4$, demonstrating that the choice of metal also has some influence over the bandgap energy [1].

Though $C_7H_7BiX_4$, $C_7H_7SbX_4$, and $C_7H_{72}PbI_6$ have been reported to show desirable primary electronic transitions, they do not demonstrate optically addressable emission suitable for use as a qubit. Adjusting the organic cation present has been shown to influence the light emission in hybrid halide materials [2], leading to the investigation of the effect of substituting 4-amino-1,2,4-triazolium (4AMTZ) for tropylium as the organic spacer cation in the bismuth iodide hybrid semiconductor. $4AMTZBiI_4$, reported in Chapter 2, shows a primary charge transfer occurring between the inorganic bismuth iodide states and the 4AMTZ π^* states. While the desired charge transfer is present in this material, $4AMTZBiI_4$ does not show optically addressable emission. Here, we use the same synthetic method reported for $4AMTZBiI_4$ in Chapter 2 to synthesize the hybrid halide materials $4AMTZBiBr_4$ and $4AMTZBiCl_4$ and measure their optoelectronic properties. We expect there to be a systematic shift in the bandgap energy between these halide congeners as has been observed in $C_7H_7BiX_4$. Potentially, swapping the halides may result in optically addressable bandgap emission.

3.2 Experimental

3.2.1 Starting Materials

Bismuth(III) oxychloride (98%, Sigma Aldrich), tropylium tetrafluoroborate (97%, Alfa Aesar), 4-amino-1,2,4-triazole (99%, Sigma Aldrich), hydrochloric acid (37%, ACS reagent, Sigma Aldrich), hydrobromic acid (48%, Alfa Aesar), acetic acid (glacial, certified ACS, Fisher Chemical), and ethyl ether (anhydrous, Fischer Chemical) were purchased from stated commercial suppliers and used without further purification.

3.2.2 Synthesis of 4AMTZ Bismuth Bromide

Bismuth(III) oxychloride (2.1 g, 8.0 mmol) was added to 5.0 mL hydrochloric acid and stirred at room temperature until dissolved to make Bi^{3+} stock solution (1.6 mM). 4AMTZ (0.72 g, 8.5 mmol) was added to 2 mL hydrochloric acid and stirred at room temperature until dissolved. Upon addition of the two clear colorless solutions a pale yellow solid began forming. Acetic acid (2.0

mL) was used as an antisolvent to increase yield. The resulting pale yellow solid was filtered, washed with ethyl ether, and dried under vacuum at room temperature overnight.

3.2.3 Synthesis of 4AMTZ Bismuth Chloride

Bismuth(III) oxychloride (2.38 g, 9.1 mmol) was added to 6 mL hydrochloric acid and stirred at room temperature until dissolved to make Bi^{3+} stock solution (1.5 mM). 4AMTZ (1.28 g, 15 mmol) was added to 3.0 mL hydrochloric acid and stirred at room temperature until dissolved. Upon additon of the two clear colorless solutions a cloudy white layer began forming on top of a clear colorless layer. Addition of acetic acid to the solution increased the size and cloudiness of the white layer. Extracting the white layer and adding 10 mL ethyl ether resulted in the precipitation of a white solid. The solid was filtered, washed with ethyl ether, and dried under vaccuum at room temperature overnight.

3.2.4 Powder X-ray Diffraction

Powder X-ray diffraction measurements were carried out using a Bruker D8 DaVinci Diffractometer with a Cu Kα radiation source and LYNXEYE-EX-T energy discriminating detector. Samples were prepared using a zero diffraction silicon wafer. Powder samples were dusted over a small amount of petroleum jelly. TOPAS software was used to refine the data based on the crystal structure of 4AMTZBiI_4 reported in Chapter 2 as the orthorhombic space group $Pbca$ (No. 61).

3.2.5 Photoluminescence Spectroscopy

An Edinburgh FS5 spectrofluorometer with a 150 W xenon lamp light source was used for all photoluminescence spectroscopy measurements. The excitation and emission monochromator range was 200 - 1000 nm and the emission detection range was 230 - 870 nm. A solid sample holder was used for room temperature measurements. For low temperature (T=77 K) measurements, the solid sample was placed in a thin wall quartz EPR sample tube before being slowly inserted into a low temperature sample stage filled with liquid nitrogen.

3.3 Powder X-ray Diffraction

Powder X-ray diffraction data taken on powdered single crystals of 4AMTZ bismuth chloride and 4AMTZ bismuth bromide are not consistent with the crystal structure of 4AMTZBiI$_4$ (Figure 3.1). Likely, the disagreement in the collected powder X-ray data and the crystal structure is due to the chloride and bromide congeners each adopting a different structure than the iodide congener. The reduced size of the halogens may affect the tilt and distortion of the inorganic octahedra, which may contribute to different positions of relatively heavy atoms that dictate the diffraction pattern. Additionally, it is possible that the powdered crystal samples contain different distinct compositions and polymorphs, as was seen in the bulk powder samples of 4AMTZBiI$_4$.

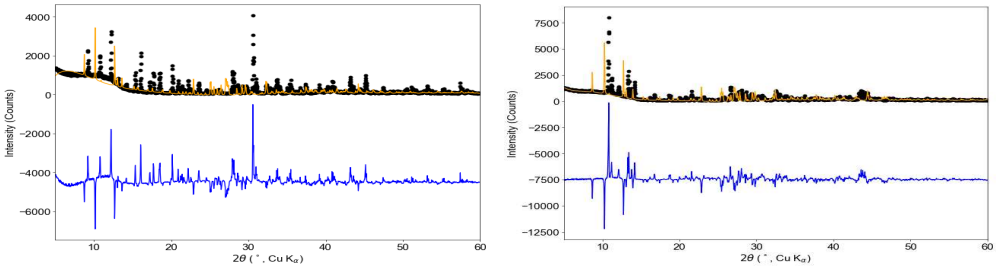

Figure 3.1: Powder X-ray diffraction patterns for powdered crystals of 4AMTZ bismuth choride (left) and 4AMTZ bismuth bromide (left). The black dots show the data, the orange line shows the fit, and the blue line shows the difference curve.

3.4 Photoluminescence Studies

The photoluminescence emission spectra of the hybrid semiconductors 4AMTZBiBr$_4$ and 4AMTZBiCl$_4$ (Figure 3.2) show two distinct regions of emission at T = 77 K. The bromide containing species (blue) emits from 425 nm - 525 nm with a lower energy region of emission from 530 nm - 800 nm. The higher energy region of emission from the chloride containing species (orange) is blue shifted relative to that of the bromide containing species, emitting from 375 nm - 450 nm. This shift in energy is expected for emission stemming from the electron transfer across a bandgap where the valence band maximum is composed primarily of halide states. The energy difference between the

halide frontier state and the organic frontier state should be larger for the chloride states than for the bromide states, resulting in higher energy emission.

A second region of emission is observed from 530 nm - 800 nm for both the chloride and bromide species. Due to the lack of energy shift in this region, this emission is not due to frontier states but could reasonably be due to a self trapped exciton (STE) localized on the inorganic lattice. A STE is formed when a bound electron-hole pair in its excited state induces distortions in the inorganic octahedra and becomes "trapped" in a quantum energy well as a result of this distortion. Because the emission from a self trapped exciton is dependent on the energy of the quantum well it is trapped in and not the frontier orbitals the emission energy is not affected by the species of halide present on the octahedra, but is more dependent on the octahedral tilt angle. Emission from STE is observed in some perovskites and their derivatives, and can be tuned by manipulating the tilt angle of the inorganic octahedra the STE is localized on [2, 17].

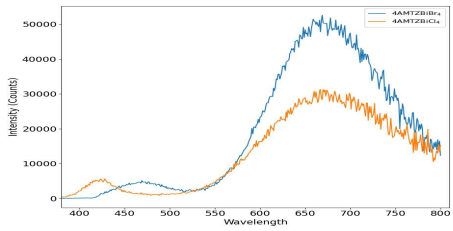

Figure 3.2: Photoluminescence spectra of 4AMTZBiBr$_4$ (blue) and 4AMTZBiCl$_4$ (orange) at T=77K.

The excitation spectra for 4AMTZBiBr$_4$ and 4AMTZBiCl$_4$ shows the optimal wavelengths that may be used to populate the excited sates of the material. As is consistent with the shift in emission energy observed from 4AMTZBiCl$_4$ and 4AMTZBiBr$_4$ in Figure 3.2, the chlorine containing species shows an excitation peak at 360 nm, blue shifted relative to the excitation from the bromine containing version at 410 nm.

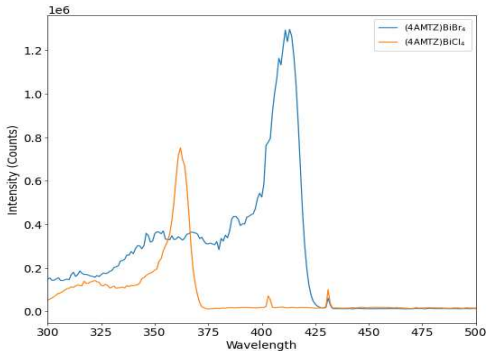

Figure 3.3: Photoluminescence excitation spectrum of $4AMTZBiBr_4$ (blue) and $4AMTZBiCl_4$ (orange) at T=77K.

3.5 Conclusion and Outlook

The structure of $4ATMZBiBr_4$ and $4AMTZBiCl_4$ remains undetermined, though, it is reasonable to assume that these congeners will have a similar structure to $4AMTZBiI_4$, but may have slightly different positioning of the inorganic octahedra due to reduced halide size. Likely, these materials are also charge-transfer semiconductors with the electronic transition occurring between the organic and inorganic layers as evidenced by the blue shifted emission from the chloride congener relative to the bromide congener at T= 77K. The evidence of a self trapped exciton in the low temperature emission spectrum shows that $4AMTZBiBr_4$ and $4AMTZBiCl_4$ demonstrate optically addressable emission from a quantum two-level system. Though this type of emission is necessary for a qubit, further studies with ODMR are complicated due to the low temperature this emission occurs at. Further studies should include definitive characterization of the bulk powder samples including single crystal X-ray diffraction, as well as tuning of octahedral tilt angle via adjustment of the organic spacer cations, which could result in a material that shows emission from a self-trapped exciton at room temperature.

Bibliography

[1] Iain W. H. Oswald, Eve M. Mosure, Ian P. Moseley, Ahn Hyochul, and James R. Neilson. Hybrid Charge-Transfer Semiconductors: $(C_7H_7)SbI_4$, $(C_7H_7)BiI_4$, and Their Halide Congeners. *Inorg. Chem.*, 58(9):5818–5826, 2019.

[2] M. Smith, B. Connor, and H. Karunadasa. Tuning the luminescence of Layered Halide Perovskites. *Chem. Reviews*, 119(5):3104–3139, 2019.

[3] Zhi-Gang Yu. Optical deformation potential and self-trapped excitons in 2D hybrid perovskites. *Royal Society of Chemistry*, 21(40):22293–22301, 2019.

[4] David P. DiVincenzo. The Physical Implementation of Quantum Computation. *Fortschritte der Physik*, 48(9-11):771–783, 2000.

[5] M. V. Gurudev Dutt, L. Childress, L. Jiang, M.D. Lukin, and et al. Quantum Register Based on Individual Electronic and Nuclear Spin Qubits in Diamond. *Science (New York, N.Y.)*, 316:1313–1316, 2007.

[6] Stephen Von Kugelgen, Matthew D Krzyaniak, Mingqiang Gu, Danilo Puggioni, James M Rondinelli, Michael R Wasielewski, and Danna E Freedman. Spectral Addressability in a Modular Two Qubit System. *Journal of the American Chemical Society*, 143(21):8069–8077, 2021.

[7] Majed S. Fataftah and Danna E. Freedman. Progress Towards Creating Optically Addressable Molecular Qubits. *Chemical Communications*, 54(98):13778–13781, 2018.

[8] Michael J. Graham, Joseph M. Zadrozny, Majed S. Fataftah, and Danna E. Freedman. Forging Solid-State Qubit Design Principes in a Molecular Furnace. *Chemistry of Materials*, 29(5):1885–1897, 2017.

[9] Nguyen T. Son, Christopher P. Anderson, Alexandre Bourassa, Kevin C. Miao, and et al. Developing silicon carbide for quantum spintronics. *Applied Physics Letters*, 116(19):190501, 2020.

[10] S. Michaelis De Vasconcellos, S. Gordon, M. Bichler, T. Meier, and A. Zrenner. Coherent control of a single exciton qubit by optoelectronic manipulation. *Nature Photonics*, 4(8):545–548, 2010.

[11] N.Y. Kim and Y. Yamamoto. *Quantum Simulators with Photons and Polaritons*, pages 91–121. Springer International, 2017.

[12] C. E. Bradley, J. Randall, M. H. Abobeih, and R. C. Berrevoets. A Ten-Qubit Solid-State Spin Register with Quantum Memory up to One Minute. *Physical Review X*, 9(3):31045, 2019.

[13] B.E. Kane. A silicon-based nuclear spin quantum computer. *Nature*, 393:133–137, 1998.

[14] Kouichi Ichimura. A simple frequency-domain quantum computer with ions in a crystal coupled to a cavity mode. *Optics Communications*, 196:119–125, 2001.

[15] D. Carbonera. Optically detected magnetic resonance (ODMR) of photoexcited triplet states. *Photosynth Res*, 102:403–414, 2009.

[16] Annalise E. Maughan, Joshua A. Kurzman, and James R. Neilson. Hybrid Inorganic-Organic Materials with an Optoelectronically Active Aromatic Cation: $(C_7H_7)_2SnI_6$ and $C_7H_7PbI_3$. *Inorg. Chem.*, 54(1):370–378, 2015.

[17] J. Thomaz, H. Lindquist, and H. Karunadasa. Single Ensemble Non-exponential Photoluminescent Population Decays from a Broadband White-Light-Emitting Perovskite. *J. Am. Chem. Soc.*, 142(39):16622–16631, 2020.